

# A three-dimensional numerical study and comparison between the air side model and the air/water side model of a plain fin-and-tube heat exchanger

R. Borrajo-Peláez<sup>a</sup>, J. Ortega-Casanova<sup>b,\*</sup>, J.M. Cejudo-López<sup>a</sup>

<sup>a</sup>Departamento de Máquinas y Motores Térmicos, Universidad de Málaga, E.T.S. Ingenieros Industriales. Calle Dr. Ortiz Ramos, 29071 Málaga, Spain

<sup>b</sup>Departamento de Ingeniería Mecánica y Mecánica de Fluidos, Universidad de Málaga, E.T.S. Ingenieros Industriales. Calle Dr. Ortiz Ramos s/n, 29071 Málaga, Spain

## ARTICLE INFO

### Article history:

Received 6 March 2009

Accepted 16 March 2010

Available online 31 March 2010

### Keywords:

3D numerical simulation

Fin-and-tube

Heat exchanger

Water and air flow

## ABSTRACT

CFD is becoming an important heat exchanger research technique. It constitutes an inexpensive prediction method, avoiding the need of testing numerous prototypes. Current work in this field is mostly based on air flow models assuming constant temperature of fin-and-tube surface. The purpose of this paper is to present an enhanced model, whose innovation lies in considering additionally the water flow in the tubes and the conduction heat transfer through the fin and tubes, to demonstrate that the neglect of these two phenomena causes a simulation result accuracy reduction.

3-D Numerical simulations were accomplished to compare both an air side and an air/water side model. The influence of *Reynolds* number, fin pitch, tube diameter, fin length and fin thickness was studied. The exchanger performance was evaluated through two non-dimensional parameters: the air side *Nusselt* number and a friction factor. It was found that the influence of the five parameters over the mechanical and thermal efficiencies can be well reported using these non-dimensional coefficients. The results from the improved model showed more real temperature contours, with regard to those of the simplified model. Therefore, a higher accuracy of the heat transfer was achieved, yielding better predictions on the exchanger performance.

© 2010 Elsevier Ltd. All rights reserved.

## 1. Introduction

In the last three decades, several studies have been carried out to characterize the heat transfer and pressure drop in tube banks and fin-and-tube heat exchangers. Focusing on the interest of this document, a brief description of the newest numerical parametric work is remarked. Romero-Méndez et al. [7] examined the influence of fin spacing on the over-tube side of a single-row fin-tube heat exchanger through flow visualization and numerical computation. The progress of the flow pattern with the non-dimensional fin spacing is observed. For low values of the parameter, the flow is Hele-Shaw. As it is increased, a horseshoe vortex is formed upstream of the tube, occurring a peak in the *Nusselt* number. In the wake region, the *Nusselt* number is very small but increases when there is fluid exchange with that downstream.

3-D Numerical simulations were performed for laminar heat transfer and fluid flow of plate fin-and-tube heat exchanger by He et al. [3]. The influences of *Reynolds* number, fin pitch, tube row number, spanwise tube pitch and longitudinal tube pitch were

examined. The results were evaluated by using the synergy principle: the strength of convective heat transfer is valued, not only by considering the local velocity vector and the temperature gradient, but also observing the synergy between them. It is found that the enhancement or deterioration of the convective heat transfer across the finned tube banks is inherently related to the variation of the intersection angle between the velocity and the fluid temperature gradient.

Later papers by the same authors undertook simulations on similar 3-D models, including geometric improvements and analyzing their influence by using the synergy principle. One of the conventional methods for enhancing the air side heat transfer is the adoption of wavy fins, which present a corrugated surface, increasing the fin surface per length unit, and therefore allowing a higher heat exchange on the fins. In 2006, 3-D numerical simulations were performed for wavy fin-and-tube heat exchangers [9]. Four factors were studied: *Reynolds* number, fin pitch, wavy angle and tube row number. The results showed that increasing wavy angles, and decreasing the fin pitch and tube row number, the heat transfer of the finned tube bank is enhanced with some penalty in pressure drop. The effects of the four parameters are well described by means of the synergy principle. Although this paper deals with 3D fin-and-tube heat exchangers, recently, this geometry has been

\* Corresponding author. Tel.: +34 951 952 382.

E-mail address: [jortega@uma.es](mailto:jortega@uma.es) (J. Ortega-Casanova).

**Nomenclature**

$A$	thermal transfer surface area ( $\text{m}^2$ )
$C_p$	specific heat ( $\text{J/kg K}$ )
$D$	tube diameter (m)
$v^2/2$	kinetic energy ( $\text{J/kg}$ )
$\vec{F}$	force vector (N)
$\rho \vec{g}$	gravitational body force (N)
$h$	enthalpy ( $\text{J/kg}$ )
$h_s$	sensible enthalpy of solid ( $\text{J/kg}$ )
$K$	air thermal conductivity ( $\text{W/m K}$ )
$K$	solid thermal conductivity ( $\text{W/m K}$ )
$L$	fin length (m)
$\dot{m}$	air mass flow ( $\text{kg/s}$ )
$P$	pressure (Pa)
$P_{\text{atm}}$	atmospheric pressure (Pa)
$P_{\text{est}}$	static pressure (Pa)
$t$	time (s)

$T_{\text{in}}^A$	air inlet temperature (K)
$T_{\text{in}}^W$	water inlet temperature (K)
$T_{\text{out}}^A$	mass-weighted average temperature of air outlet grid cells where backflow does not occur (K)
$T_{\text{out}}^W$	mass-weighted average temperature of water outlet grid cells where backflow does not occur (K)
$T_w$	wall average temperature (K)
$T_s$	solid temperature (K)
$u, v, w$	$x, y, z$ velocity components (m/s)
$U_c$	maximum air velocity at minimum cross-sectional area (m/s)
$U_{\text{in}}$	air inlet velocity (m/s)
$\vec{v}$	velocity vector (m/s)
$V_{\text{in}}$	water inlet velocity (m/s)
$\mu$	air viscosity ( $\text{kg/m s}$ )
$\rho$	air density ( $\text{kg/m}^3$ )
$\rho_s$	solid density ( $\text{kg/m}^3$ )
$\frac{\rho_s}{\tau}$	shear stress tensor (Pa)

successfully modeled as a one-dimensional circuit [2], obtaining good results, with differences less than 1% with respect to the higher dimension problem.

Another conventional method for improving the air side heat transfer is the use of plain plate fins and elliptic tubes heat exchanger, which were studied experimentally by Jang and Yang [5], and Saboya and Saboya [8]. These papers showed that elliptic tubes present a better heat transfer than circular ones. Matos et al. [6] performed 2-D heat transfer analyzes of non-finned circular and elliptic tubes heat exchangers. Numerical results showed a relative heat transfer improvement of around 13% in the optimal elliptical arrangement, with regard to the circular one. In 2007, wavy fin heat exchangers with elliptic-circular tubes were considered by Tao et al. [10]. Circular and elliptic arrangements with the same minimum flow cross-sectional area were compared. A maximum relative heat transfer gain of up to 30% is observed in the elliptic arrangement, and the corresponding friction factor only increased by about 10%.

The foregoing numerical documentation only analyzes the air side flow of the heat exchanger. The aim of this paper is to demonstrate that there exists a difference between the results obtained from a simplified model, where only the air flow is taken into account, and the results obtained from a complex one where, together with the air flow, the water flow through the tubes and the heat flux along the fin and tubes are solved too.

The influence of five parameters is studied:  $Re$  number, fin pitch, tube diameter, fin length and fin thickness. Firstly, 3-D numerical simulations are performed on air side models. A constant temperature on the walls is imposed through the boundary conditions, to simulate the effect of the cold water in the heat exchanger. Afterwards, the model is provided with a greater complexity, so that the water flow and the fin-and-tube heat fluxes are considered in the computation domain. The trends of the non-dimensional coefficients with regard to every parameter variation are compared for both models. It is found that considerable differences exist between the results of the simple and the complex model.

## 2. Model description

### 2.1. Physical model

A view of a single row fin-and-tube heat exchanger is showed in Fig. 1. Due to limitations on the computing resources, only the minimum portion of the heat exchanger able to describe the flows was taken as a calculation element, assuming the existence of

symmetry in the  $y$ -direction, perpendicular to the fin surface, and periodicity in the  $z$ -direction. Fig. 2 presents the selected part of the two row heat exchanger.

In Fig. 3, the dimensions and zones of the final model are illustrated. Table 1 shows the dimensions of the model, which have been chosen according to the dimensions of standard heat exchangers observed in air-conditioning. Two additional zones are considered in the computational domain: an inlet zone to study the incidence of the air flow over the fin, and an outlet one, to minimize the backflow during the simulations. The mesh is divided into different zones, as shown in Fig. 3, so that the distortion of the elements that form the grid is minimized, since distortion implies a very bad influence on the convergence, the stability and the computing time of the numerical simulations. It also allows the use of different element density in each zone, depending on the gradient of the fluid magnitudes appearing in each region of the domain, achieving computational saving in the solution of the problem. Boundary layers are arranged on the tube and fin surfaces, as well as on the entry and exit surfaces of the space between two fins.

### 2.2. Flow considerations

Some assumptions to simplify the flow have been taken into account. The fluids are considered to be incompressible, with

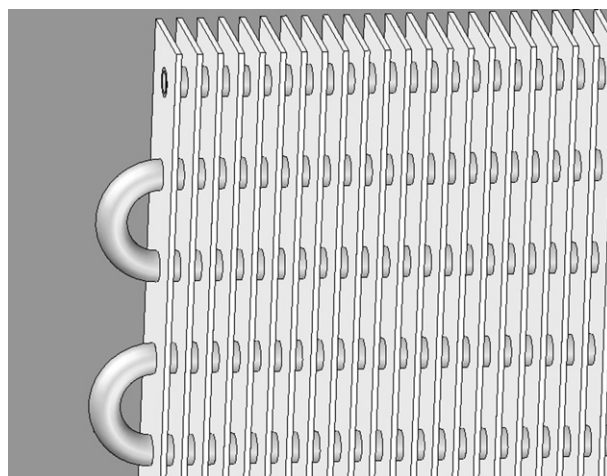


Fig. 1. View of a single row fin-and-tube heat exchanger.

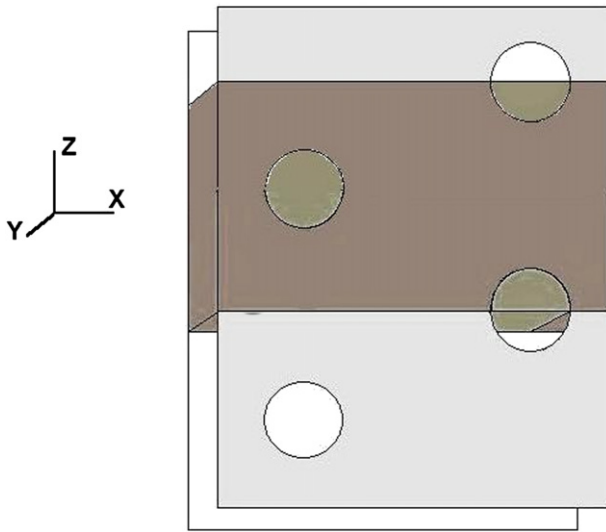


Fig. 2. Computation domain of the two row fin-and-tube heat exchanger.

Table 1  
Model measures.

Measure	Length (mm)
Inlet (I)	10
Outlet (O)	30
Height (H)	25
Fin length (FL)	21.65
Tube diameter (TD)	10.55
Fin pitch (FP)	2
Fin thickness (FT)	0.15

regime (see ref. [3], among others), justifying the usage of laminar steady models in the good results obtained by many similar numerical studies in comparison to experimental data for *Reynolds* number greater than 1000 [5]. In addition, other authors have concluded that, when the flow reaches periodic unsteady regime in corrugated channels, it is appropriate to use a steady model to predict the averaged *Nusselt* number and friction factor, and the usage of an unsteady model is not necessary since the unsteady model provides almost the same *Nusselt* number and friction factor as the steady model [11].

A mesh convergence analysis to determine the effect of the mesh elements size was carried out. Successive simulations were performed, increasing the mesh element density, to observe the *Nusselt* number trend. In this analysis, successive models were built, varying the number of elements in every direction independently. The number of elements in *x*-direction varied between 94 and 262. The *Nusselt* number showed a constant trend for more than 173 elements, so this is the optimal resolution in this direction. For *y*-direction, the number varied between 15 and 85, and the optimal number of elements is 45. Finally, for *z*-direction, the number of nodes ranged from 10 to 80, and the *Nusselt* number reached a constant trend for 50 elements. From the result of this analysis, it is concluded that the optimal mesh is the one formed by  $(173 \times 45 \times 50)$  elements, more than  $5 \times 10^5$  nodes. When varying the model dimensions during the parametric study, the domain was meshed so that the density was similar to the one obtained for the optimal grid.

### 2.3. Governing equations

FLUENT 6.2 is the software used to perform the simulations on this paper. Its code is based on the Finite Volume Method, consisting in the discrete approximation of the volume and surface integrals of the Navier–Stokes equations in steady state, applied to each control volume, in whose center, a computational node is

homogeneous constant properties. The steady state of the flow is studied. The air *Reynolds* number for the simulations performed in this work ranges between 500 and 5000, while the water *Reynolds* number, based on the water properties, tube diameter and flow rate through it, remains constant and equal to 6300. The air *Reynolds* number will be referred to in the following as the *Reynolds* number. Currently, there is not a fixed criterion to determine whether the flow through a finned tube bank is laminar or turbulent. However, there exist references for simpler cases. According to certain experimental data, transition from laminar to turbulent flow takes place for *Reynolds* number around 2300 in parallel surface confined flows (*Re* based on the double distance between surfaces, [4]). For cylinders in cross flow, the limit has been observed to appear at *Reynolds* number close to  $2 \times 10^5$  (*Re* based on the tube diameter, [4]). In the movement of a fluid between two close surfaces, the flow is considered to be laminar if the viscosity forces are dominant compared to the inertia forces, which means that the following conditions must be fulfilled:  $[h/L \ll 1]$  and  $[Re(h/L) \ll 1]$ , being *h* and *L* characteristic lengths in the cross and longitudinal direction of the flow, respectively [1]. The first condition is satisfied for every case studied in this paper, but the second one is not fulfilled for the higher *Reynolds* number cases. However, previous work on similar 3-D simulations have posed the same question about the flow

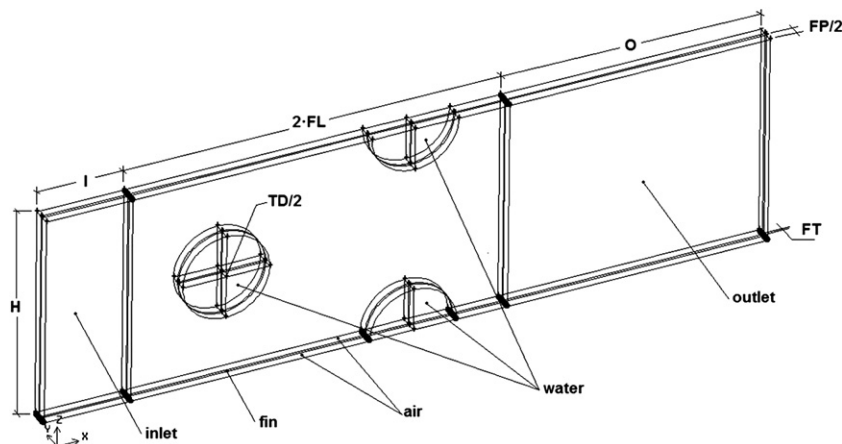


Fig. 3. Geometric model dimensions and zones.

placed. The continuity, momentum and energy partial differential equations solved by the software are, respectively,

$$\frac{\partial \rho}{\partial t} + \nabla \cdot (\rho \vec{v}) = 0, \quad (1)$$

$$\frac{\partial}{\partial t}(\rho \vec{v}) + \nabla \cdot (\rho \vec{v} \vec{v}) = -\nabla p + \nabla \cdot (\bar{\tau}) + \rho \vec{g} + \vec{F}, \quad (2)$$

$$\frac{\partial}{\partial t}(\rho E) + \nabla \cdot (\vec{v}(\rho E + p)) = \nabla \cdot (k \nabla T + (\bar{\tau} \cdot \vec{v})), \quad (3.1)$$

where

$$E = h - \frac{p}{\rho} + \frac{v^2}{2}. \quad (3.2)$$

For the air/water model, the temperature distribution inside the solid regions of the model, such as tube walls and fin, is obtained by Fluent solving the energy equation

$$\frac{\partial}{\partial t}(\rho_s h_s) = \nabla \cdot (k_s \nabla T_s). \quad (4)$$

This equation will allow us to obtain the temperature, not only inside the fin, but also along its surface, in order to get the average Nusselt number on it.

## 2.4. Boundary conditions

### 2.4.1. Air side simulations

For the case that only considers the air side flow, the boundary conditions for velocity, pressure and temperature are the following:

#### - Velocity and Pressure:

Air Inlet boundary:  $u = U_{in}$ ,  $v = w = 0$ ;

Air Outlet boundary:  $P_{est} = P_{atm}$ ;

Upper side and lower side: Periodicity;

Left side and right side: Symmetry ( $\partial u / \partial y = 0$ ,  $\partial v / \partial y = 0$ ,  $\partial w / \partial y = 0$ );

Tube and fin walls:  $u = v = w = 0$ ;

#### - Temperature:

Air Inlet boundary:  $T = T_{in}^A$ ;

Air Outlet boundary:  $T = T_{out}^A$ ; (It applies only to the grid cells where backflow occurs)

Left side and right side: Symmetry ( $\partial T / \partial y = 0$ );

Tube and fin walls:  $T = T_w$ ;

### 2.4.2. Air and water side simulations

For the complex case, that also takes into account the water side flow and the heat transfer through the fin, it is necessary to introduce some additional boundary conditions for the water flow:

#### - Velocity and Pressure:

Air Inlet boundary:  $u = U_{in}$ ,  $v = w = 0$ ;

Water Inlet boundary:  $v = V_{in}$ ,  $u = w = 0$ ;

Air Outlet boundary:  $P_{est} = P_{atm}$ ;

Water Outlet boundary:  $P_{est} = P_{atm}$ ;

Upper side and lower side: Periodicity;

Left and right air side: Symmetry ( $\partial u / \partial y = 0$ ,  $\partial v / \partial y = 0$ ,  $\partial w / \partial y = 0$ );

Tube and fin walls:  $u = v = w = 0$ ;

#### - Temperature:

Air Inlet boundary:  $T = T_{in}^A$ ;

Water Inlet boundary:  $T = T_{in}^W$ ;

Air Outlet boundary:  $T = T_{out}^A$ ; (It applies only to the grid cells where backflow occurs)

Water Outlet boundary:  $T = T_{out}^W$ ; (It applies only to the grid cells where backflow occurs)

Left side and right side: Symmetry;  $\partial T / \partial y = 0$ ;

tube and fin walls: Coupled Walls (in Fluent terminology); (Fluent calculates the heat fluxes. It is not necessary to impose any BC)

The numerical values of the foregoing variables are the following:  $U_{in} = 1.4$  m/s;  $P_{atm} = 101\,300$  Pa;  $V_{in} = 0.6$  m/s;  $T_{in}^A = 300$  K;  $T_{in}^W = 280$  K;  $T_w = 280$  K. Backflow takes place at some of the nodes in the flow outlet surfaces. A constant temperature value can be set by Fluent user for fluids in the Backflow nodes. However, to avoid the arbitrary selection of temperature in these nodes, which would lead to distortion of solution data obtained from simulations, a Fluent User Defined Function is used to automatically change the temperature assigned to backflow nodes depending on the evolution of temperature in all the nodes of the outlet surface. This function detects the nodes in which backflow does not occur, calculates their mass-weighted average temperature ( $T_{out}^A$  and  $T_{out}^W$ ) and, assuming that the temperature of backflow fluid is close to the average temperature of the outgoing flow, assigns this value to the nodes affected by backflow.

Since the water temperature is lower than the air temperature, the air is cooled. The temperature of the tube and fin metal surfaces is very close to the water temperature because the heat transfer coefficient between water and metal is high. Normally, this temperature is lower than the dew point of the air moisture, so the condensation of air moisture takes place on the metal surface of the heat exchanger. This effect has been neglected in this work, considering that the air that circulates through the heat exchanger does not contain water vapour.

## 3. Results and discussion

The results of examining the effect of the *Reynolds* number, fin pitch, tube diameter, fin length and fin thickness are analyzed and compared for both the air side model and the air/water side model. While varying each of the foregoing parameters, the others remain invariable.

### 3.1. Non-dimensional parameters

From the numerical results, the thermal performance of the heat exchanger was judged according to a non-dimensional parameter: the air side *Nusselt* number, defined as follows:

$$Nu = \frac{h \cdot D}{K}, \quad (5)$$

where  $h$  is the convective heat coefficient for air, based on the heat flux from the air to the heat exchanger  $Q$ , and the log-mean temperature difference  $\Delta T$ :

$$h = \frac{Q}{A \cdot \Delta T},$$

$$Q = \dot{m} \cdot C_p \cdot (\bar{T}_{in} - \bar{T}_{out}), \quad \Delta T = \frac{(T_w - \bar{T}_{in}) - (T_w - \bar{T}_{out})}{\ln[(T_w - \bar{T}_{in}) / (T_w - \bar{T}_{out})]},$$

where  $\bar{T} = \iint u \cdot T \cdot dA / \iint u \cdot dA$  is the average temperature evaluated on a surface.

Regarding to the mechanical performance, the criteria chosen was a friction coefficient:

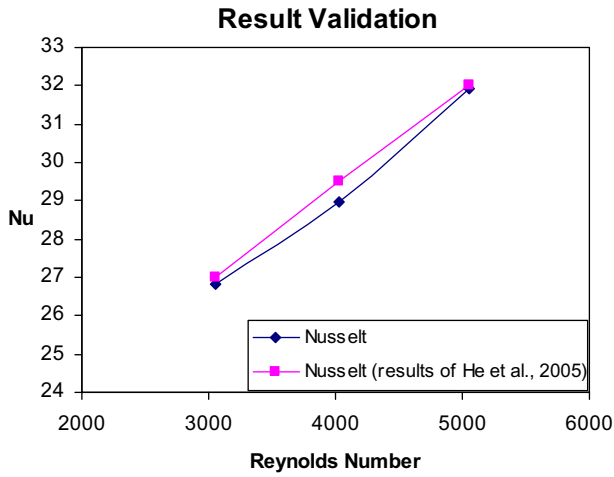


Fig. 4. Variation of Nu with Re (comparison with results of [3]).

$$FC = \frac{\Delta P \cdot D}{(1/2) \cdot \rho \cdot U_c^2 \cdot L} \quad (6)$$

where  $\Delta P = \bar{P}_{in} - \bar{P}_{out}$  is the pressure drop across the heat exchanger, considering the average pressure:

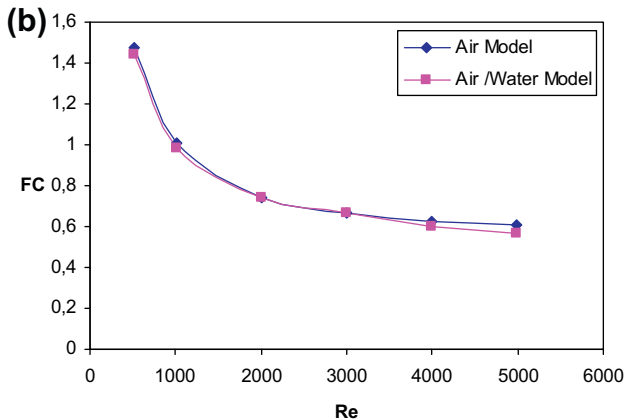
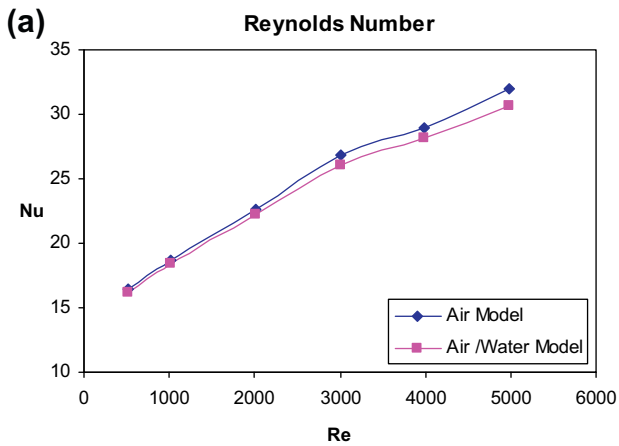


Fig. 5. Variation of Nu (a) and FC (b) with Re

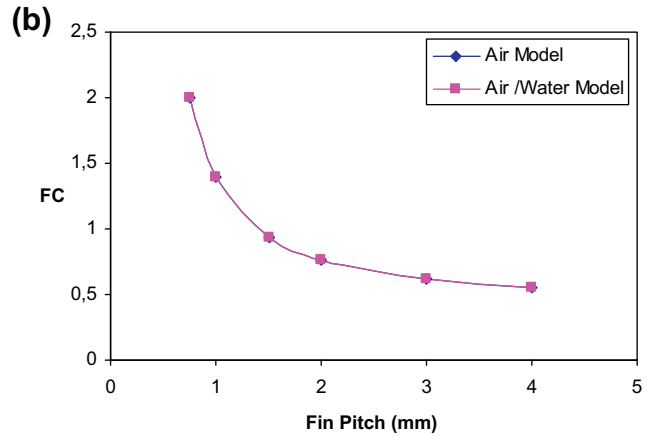
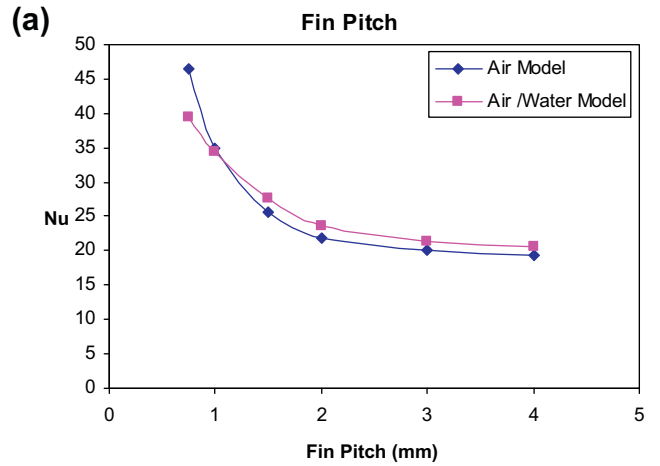


Fig. 6. Variation of Nu (a) and FC (b) with Fin Pitch.

$$\bar{P} = \frac{\iint_A P \cdot dA}{\iint_A dA}$$

The Reynolds number is based on the air properties and is definded as

$$Re = \rho U_c D / \mu$$

### 3.2. Model Validation

To check the model validity, a model with the same size and operating conditions as the one employed in He et al. [3] was built. Simulations for a wide range of Reynolds number were performed, as shown in Fig. 4, where a good agreement between the results obtained with both models is observed, being the differences between the Nusselt numbers calculated for each Reynolds number less than 1.75%.

### 3.3. Reynolds number effect

For the simulations performed in this section, the air Reynolds number varies between 500 and 5000, ranging the air inlet velocity between 0.4 and 4 m/s Fig. 5(a) shows the variation of Nusselt number, increasing when the inlet velocity is raised. It means that the increase in the Reynolds number yields an improvement in the convection heat transfer of the heat exchanger, and thus, an enhancement of the device performance. Comparing the results for the air side model and the air/water side model, it can be observed

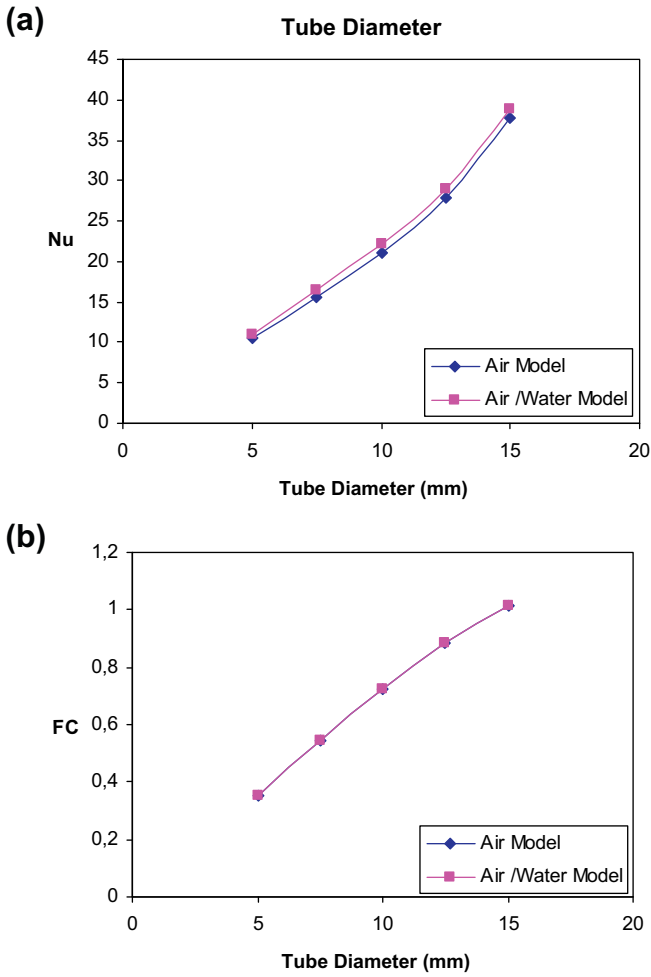


Fig. 7. Variation of  $Nu$  (a) and  $FC$  (b) with Tube Diameter.

that the *Nusselt* number predicted by the latter is slightly lower. The difference grows as the inlet velocity increases. The Friction Coefficient, as shown in Fig. 5(b), decreases as the Reynolds number increases, however, it is not possible to state that the mechanical performance of the device can be improved by raising the inlet velocity, since the pressure drop across the exchanger, that depends on the dynamic pressure too, increases with air inlet velocity. There is no difference between the results of both models in this case: mechanically, the air flow behaves identically, regardless of the water flow. This fact was also checked for the other studies carried out, that is, the Friction Coefficient gives the same curve for both the air and air/water side models.

### 3.4. Fin pitch effect

The fin pitch is varied between 0.75 and 4 mm. Reducing the separation between fins implies the existence of a greater number of fins per tube unit length and, thus, a bigger thermal contact surface area. Since the *Nusselt* number increases as the fin pitch is reduced, Fig. 6(a), the convection heat transfer is improved, which enhances the thermal performance of the heat exchanger. There are no significant differences between the results of the air and air/water side models in this case. In contrast, the Friction Coefficient grows very significantly when the space between fins is reduced, as shown in Fig. 6(b), because of the obstruction in the air flow. Therefore, the mechanical performance decreases. Again, the Friction Coefficient for both models is identical.

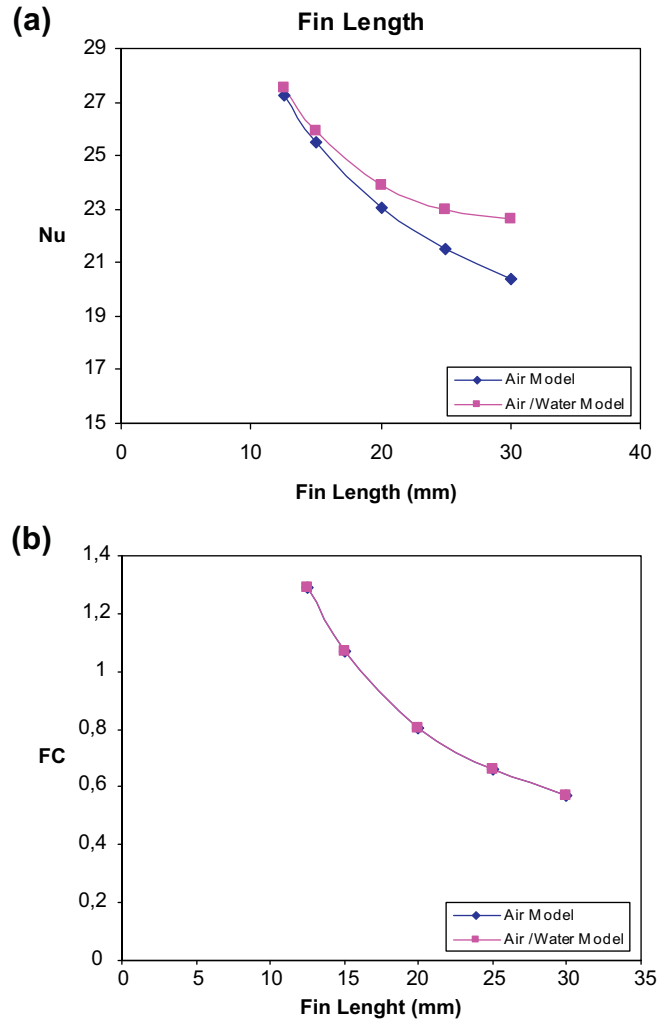


Fig. 8. Variation of  $Nu$  (a) and  $FC$  (b) with Fin Length.

### 3.5. Tube diameter effect

To study the influence of the tube diameter, this parameter is varied between 5 and 15 mm. A strong dependence of the *Nusselt* number with this factor is observed, Fig. 7(a). The value of  $Nu$  is quadrupled in the studied range. Hence, there exists a big enhancement of the convection heat transfer with the increase of the tube diameter. It can be explained by noticing that the increase of the tube diameter carries out a growth in the area of the thermal contact surface between the air and the heat exchanger. Additionally, the increase in the tube diameter permits a greater water flow across the exchanger. It allows a bigger cooling capacity of the device, and therefore, a cooler temperature profile in the metal walls, that improves the convection heat transfer. The results of the air side and the air/water side models are very similar. On the other hand, enlarging the tubes causes a worsening in the mechanical performance, since the Friction Coefficient increases, as shown in Fig. 7(b). It is due to the obstruction of the flow by the larger tubes, which produce a greater pressure drop.

### 3.6. Fin length effect

The range selected for the fin length varies between 12.5 and 30 mm. The tubes maintain their position, centered in the fin. The increase of the fin length entails a decrease in the convection coefficient. Since this coefficient is directly proportional to  $Nu$ , the

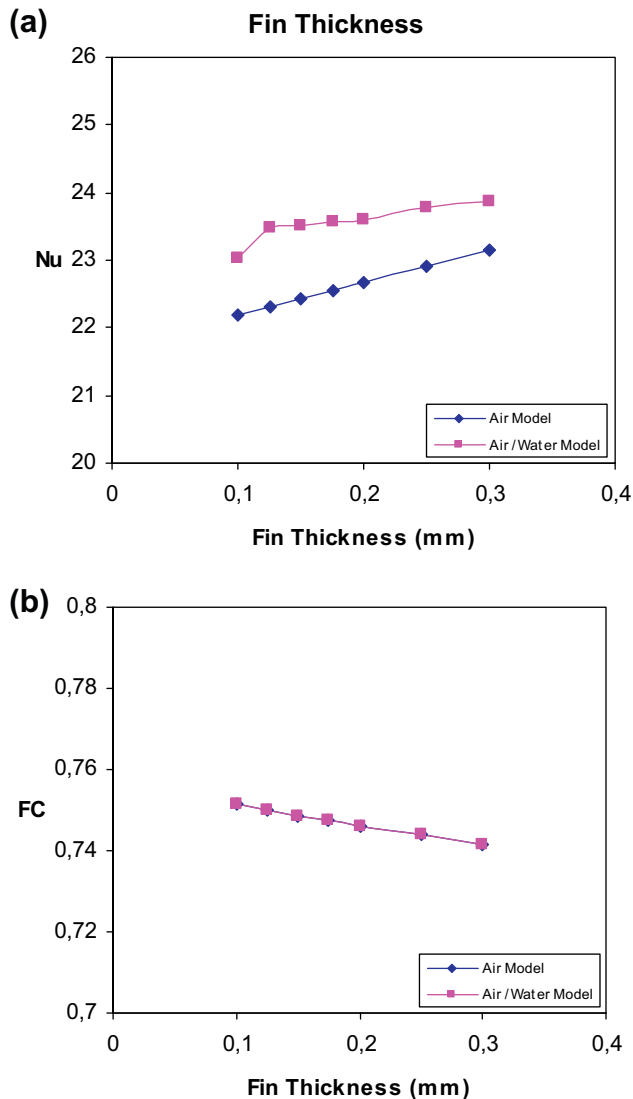


Fig. 9. Variation of  $Nu$  (a) and  $FC$  (b) with Fin Thickness.

thermal performance of the device is reduced. The air side model predicts a stronger decrease of  $Nu$ , Fig. 8(a). The increase in the fin length implies the growth of the maximum air velocity. Furthermore,  $FC$  is inversely proportional to the fin length. Thus,  $FC$  decreases as the fin length rises.

### 3.7. Fin thickness effect

Varying the fin thickness between 0.1 and 0.3 mm, a slight increase in the  $Nusselt$  number is achieved. It can be observed in Fig. 9(a) that the value for this parameter predicted by the air/water side model is around 5% higher than the one predicted by the simpler model. The results of both models follow a similar trend. Regarding the Friction Coefficient, identical results are obtained from both models, as shown in Fig. 9(b).

## 4. Conclusions

In this paper, 3-D numerical simulations are conducted to study the influence of  $Reynolds$  number ( $Re$ ), fin pitch, tube diameter, fin length and fin thickness on the air side  $Nusselt$  number ( $Nu$ ) and a friction coefficient ( $FC$ ) of a fin-and-tube heat

exchanger. The results of two different models are compared: a simpler model considering the air flow through the exchanger, and another one that also includes the water flow and the heat flux along the fin and between the air and the water. Regarding the friction coefficient, that is, the mechanical performance of the device, both models give the same results, so it is independent of both the water flow and the thermal conduction through the fin. However, the thermal performance is different depending on the model finally studied, and it is bigger when the size of the fin is varied, and it presents small differences when the other parameters are changed. In summary,

1. The increase in  $Re$  entails a growth of  $Nu$ , therefore the convection heat transfer gains importance and the heat exchanger thermal performance is enhanced. The  $Nu$  predicted by the air/water side model is slightly lower. Since  $FC$  decreases, the mechanical performance is also improved.
2. Reducing the distance between fins enhances the thermal performance of the heat exchanger, i.e., the  $Nu$  increases. There are no significant differences between the results of the air and air/water side models in this case. The  $FC$  rises intensely when reducing the fin pitch as it generates an obstruction in the air flow. Hence, the mechanical performance decreases.
3. An intense dependence of the  $Nu$  with the tube diameter is observed. Therefore, a big enhancement of the convection heat transfer with the tube diameter increase is achieved. The results of the air side and the air/water side models are very similar. However, the presence of larger tubes generates a growth of the  $FC$ , and a worsening of the mechanical performance.
4. Increasing the fin length causes a decrease of the  $Nu$ , due to the existence of a greater amount of metal which is to be cooled, and the decrease of the convective heat transfer coefficient. The reduction predicted for this parameter is lower in the case of the air/water side model. In addition, the  $FC$  is inversely proportional to the fin length. Hence, it decreases as the fin length rises.
5. The increase in the fin thickness produces a slight growth in the  $Nu$ . The value of it predicted by the air/water side model is around 5% higher than the one predicted by the simpler model, following a similar trend. Regarding the Friction Coefficient, results for both models remain almost constant when increasing the fin thickness.

With this work, the authors want to show that one has to take care with the conclusions extracted from simplified models, especially those related with the thermal performance of the device, when they are going to be used for design purposes.

## Acknowledgements

This work has been supported by AIRZONE S.L. Parque Tecnológico de Andalucía C/Marie Curie, 21 29590 Málaga – Spain

## References

- [1] G.K. Batchelor, Introduction to Fluid Dynamics. Cambridge University Press, 1967.
- [2] G. Comini, S. Savino, Accuracy of one-dimensional design procedures for finned-tube heat exchangers. Applied Thermal Engineering 29 (2009) 2863–2869.
- [3] Y.L. He, W.Q. Tao, F.Q. Song, W. Zhang, Three-dimensional numerical study of heat transfer characteristics of plain plate fin-and-tube heat exchangers from view point of field synergy principle. International Journal of Heat and Fluid Flow 26 (2005) 459–473.
- [4] F.P. Incropera, D.P. DeWitt, Fundamentals of Heat and Mass Transfer. John Wiley and Sons, 2002, 407–408, 495.

- [5] J.Y. Jang, J.Y. Yang, Experimental and 3-D numerical analysis of thermal hydraulic characteristics of elliptic finned-tube heat exchangers. *Heat Transfer Engineering* 19 (4) (1998) 55–67.
- [6] R.S. Matos, J.V.C. Vargas, T.A. Laursen, F.E.M. Saboya, Optimization study and heat transfer comparison of staggered circular and elliptic tubes in forced convection. *International Journal of Heat and Mass Transfer* 44 (2001) 3953–3961.
- [7] R. Romero-Méndez, M. Sen, K.T. Yang, R. McClain, Effect of fin spacing on convection in a plate fin and tube heat exchanger. *International Journal of Heat and Mass Transfer* 43 (1999) 39–51.
- [8] S.M. Saboya, F.E.M. Saboya, Experiments on elliptic sections in one and two-row arrangements of plate fin and tube heat exchangers. *Experimental Thermal and Fluid Sciences* 24 (2001) 67–75.
- [9] Y.B. Tao, Y.L. He, J. Huang, Z.G. Wu, W.Q. Tao, Three-dimensional numerical study of wavy fin-and-tube heat exchangers and field synergy principle analysis. *International Journal of Heat and Mass Transfer* 50 (2006) 1163–1175.
- [10] Y.B. Tao, Y.L. He, Z.G. Wu, W.Q. Tao, Three-dimensional numerical study and field synergy principle analysis of wavy fin heat exchangers with elliptic tubes. *International Journal of Heat and Fluid Flow* 28 (2007) 1531–1544.
- [11] Wei Xue, Jingchun Min, Numerical predictions of fluid flow and heat transfer in corrugated channels. in: *Proceedings of the third International Symposium on Heat Transfer and Energy Conservation*, Guangzhou, China, vol. 1, 2004, 12–15, pp. 714–21.